IEEE Access
Multidisciplinary | Rapid Review | Open Access Journal

Received October 6, 2018, accepted October 22, 2018, date of publication October 31, 2018, date of current version December 3, 2018.

Digital Object Identifier 10.1109/ACCESS.2018.2878976

Kinematic Calibration of a 2-DoF Over-Constrained Parallel Mechanism Using Real Inverse Kinematics

TAO SUN[1], (Member, IEEE), BINBIN LIAN[1,2], JIATENG ZHANG[1], AND YIMIN SONG[1], (Member, IEEE)

[1]School of Mechanical Engineering, Tianjin University, Tianjin 300350, China
[2]Mechatronics Division, Department of Machine design, KTH Royal Institute of Technology, SE-11428 Stockholm, Sweden

Corresponding author: Binbin Lian (binbin2@kth.se)

This work was supported by the National Natural Science Foundation of China under Grant 51475321, Grant 51875391, and Grant 51875392.

ABSTRACT The kinematic accuracy improvement is a key challenge in the development of over-constrained parallel mechanisms (PMs). Taking a two degree-of-freedom (DoF) over-constrained PM applied in assembly line as an example, this paper addresses the kinematic calibration problem of over-constrained PM to improve accuracy and promote its practical application. Instead of establishing conventional error mapping model, a nonlinear error model is built by inserting geometric errors of parts to the real inverse position analysis. On this basis, a set of nonlinear identification equations are formulated. Unlike other methods that identify the geometric errors by an identification Jacobian matrix and pay extra attention to the robustness of the matrix, these nonlinear identification equations are directly solved by optimization technique. Herein, the hybrid genetic algorithm is adopted in the optimization due to its high robustness, efficiency, and accuracy. Finally, error compensation is implemented by modifying the motor outputs in the controller. Simulations and experiments are then carried out to verify the calibration method, which show that the orientation accuracy of the 2-DoF over-constrained PM improves by 93.96% and 90.38%, respectively. Comparative studies to the conventional regularization method and four other optimization algorithms are also investigated. The results further confirm the high accuracy of the proposed kinematic calibration method for over-constrained PMs.

INDEX TERMS Over-constrained parallel mechanism, kinematic calibration, real inverse kinematic, hybrid genetic algorithm.

I. INTRODUCTION

Over-constrained parallel mechanism (PM) has drawn much attention from both academia and industry because it has the merit of PMs such as potentially high stiffness, large load weight ratio and good dynamic response. In the meantime, it keeps the same mobility but offers extra constraints to the end-effector, contributing to the rigidity improvement of the whole mechanism [1], [2]. One typical example is the over-constrained Delta PM for high speed pick-and-place operation in the food packaging, medicine and semiconductor manufacturing [3]. Motivated by its success, substantial researches have been carried out for further practical applications of the over-constrained PMs [4], [5].

Along this track, we developed a 2 degree-of-freedom (DoF) over-constrained PM for pose adjusting, target tracking or positioning in the assembly line. For instance, up to 90° rotation range and a rotating speed between 10° to 20° degree per second are required for the components assembling in aviation or aerospace. The proposed PM has large rotating capabilities, and the over-constrained feature is introduced for better load-carrying and higher stiffness for such application scenarios. The prototype has been built after design optimization [6]. The next problem for its practical application is the accuracy improvement, which is also a key issue for the development of over-constrained PMs regarding as potential candidates for other industrial domains.

Kinematic calibration and feedback control are recognized as two inevitable steps to improve accuracy, where the former is a necessary preparation for the latter step. Kinematic calibration improves mechanism accuracy by identifying the

geometric errors and compensating them in the controller [7]. Past few decades have witnessed the developments of PMs' kinematic calibration. Generally, it can be divided into four stages: error modeling, measurement planning, parameter identification and error compensation [8]. Kinematic calibrations of the over-constrained PMs follow the same procedure since they are the subset of PMs.

Error modeling is the formulation of linear mapping models between geometric errors of the parts and pose errors of the moving platform. The mapping matrix, named as error Jacobian matrix, is intended to be built. The pose error is calculated by linearization or differentiation of displacement equations. As a result, the mechanism errors are the linear superposition of the joint displacements and the geometric errors. Mathematical tools, such as D-H convention [9], closed-loop vector [10], screw theory [11] or POE formula [12], have been applied to the error modeling of PMs. Among them, screw theory based method is highly welcome due to the application of wrenches to exclude the passive joint twists. Especially for the over-constrained PMs, all limb wrenches, including the over-constrained wrenches, can be adopted to the formulation of error Jacobian matrix. The obtained error model is assumed to be more precise and complete [13].

Measurement planning is to use the least measuring configurations for the best identification results [14]. Then a set of identification equations are formulated to identify the geometric errors, which is called parameter identification [15]. The main challenge for these two stages is the ill-conditioning problem of the identification Jacobian matrix, which is brought by linear dependence of some geometric errors. In the conventional measurement planning of PMs, optimizations of measurement configurations are intensively investigated to increase robustness of the identification Jacobian matrix. Various observability indices and different searching methods have been proposed [16]–[18]. In the parameter identification, there are two research trends to address the ill-conditioning problem of the identification Jacobian matrix. One is to eliminate redundant errors and then solve the equations by direct inverse [19]. The other is adding regularization parameters to control the quality of the solutions [4], [16]. Since linear correlation analysis in the former trend is rather difficult for PMs, regularization methods in the latter trend have been widely adopted, for instance, the generalized cross validation method for a 3-DoF spatial PM [20] and the regularization selection method for a 2-DoF planar PM [21].

Finally, error compensation is performed by modifying the kinematic parameters in the control system according to the identified geometric errors [22]. During this process, the real kinematic models with the consideration of geometric errors are built for the following motion control. But the inputs of the over-constrained PMs cannot be derived from the actual kinematic models when assigning certain poses to the moving platform. One possible reason is that the kinematic constraints corresponding to the over-constrained features are violated because of the geometric errors. Hence, error compensation of the over-constrained PMs is usually implemented by input modifications based on the geometric error model [4], [13].

In summary, current kinematic calibration methods for the over-constrained PMs use the inverse of identification Jacobian matrix for identifying and compensating geometric errors. Extra attention has to be paid to the consideration of over-constrained features in the formulation of identification Jacobian matrix. In addition, intensive efforts are required by the measurement planning and the parameter identification for robust calibration. All these make the calibration process tedious. The improvement of accuracy is limited.

Having realized above-mentioned problems, we proposed a novel kinematic calibration method for the over-constrained PMs in this paper. Geometric error model is built by inserting the geometric errors to the inverse kinematic model. Since the inverse kinematic equations are formulated by each closed-loop, the geometric error model based on real inverse kinematics can be divided into several sub-models. Thus, the same measuring data can be applied to identify the geometric errors of each sub-model, increasing the efficiency of both measurement planning and parameter identification. In the following, a set of nonlinear equations aiming at minimizing actual and normal motor outputs are formulated. Solving nonlinear identification equations becomes the main task instead of worrying the robustness of identification Jacobian matrix. In this way, the geometric errors can be identified without implementing complicated measurement planning but adopting reliable algorithm for the nonlinear problems. Herein, a hybrid genetic algorithm (HGA) is applied, which is widely recognized as robust, accurate and efficient algorithm for dealing with nonlinear optimization problems. The details will be illustrated in the following sections.

The organization of the paper is as follow. Section II briefly introduces the 2-DoF over-constrained PM and its controlling scheme. Section III presents the geometric error modeling by real inverse kinematics, while Section IV investigates parameter identification by HGA. Simulations and experiments are implemented in Section V. Comparative studies are discussed in Section VI. Finally, conclusions are drawn in Section VII.

II. THE 2-DOF OVER-CONSTRAINED PM

The 2-DoF over-constrained PM consists of a fixed base, a moving platform, a SS limb and four symmetrically distributed RSR limbs (see Fig. 1a). Herein, R and S denote the revolute and spherical joints. The R joints linking to the fixed base in the 1st and 2nd RSR limbs are connected to torque motors. Necessary notations and coordinate frames are defined as shown in Fig. 1b. Point B_i, S_i and A_i ($i = 1, 2, 3, 4$) denote the center of joints within RSR limb in sequence. Point B_{i} and A_i are located on a circle respectively. The radiuses are both a. The lengths of the RS and SR links are all l. Point O and C_E are the centers of fixed base and moving platform. They are also the centers of S joints in SS limb. The length of SS limb is given by h. A fixed coordinate frame

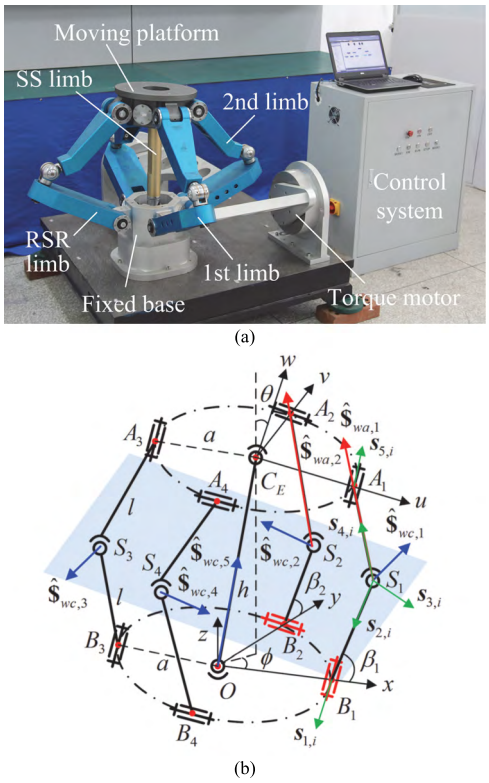

FIGURE 1. The 2-DoF over-constrained PM (a) physical prototype, (b) schematic diagram.

$O-xyz$ is assigned to point O. The x-axis is from point O to point B_1, and the z-axis is perpendicular to the fixed base. Similarly, a moving coordinate frame C_E-uvw is established at point C_E. The direction of the u-axis is from point C_E to point A_1. The w-axis is normal to the plane of the moving platform. The frames are defined according to the right hand rules.

In the framework of screw theory, the twist of point C_E can be formulated by the twists of joints within RSR limbs or SS limb as follows.

$$\$_{\mathrm{t}} = \sum_{j=1}^{5} \dot{\theta}_{\mathrm{a},j,i} \hat{\$}_{\mathrm{ta},j,i}, \quad i = 1, 2, \cdots, 5 \tag{1}$$

where $\hat{\$}_{\mathrm{ta},j,i}$ and $\dot{\theta}_{\mathrm{a},j,i}$ denote the unit twist screw and its intensity of jth 1-DoF joint in the ith limb (SS limb is described as the 5th limb). The S joint is expressed by three R joints whose axes are linear independent. Since only R joints are involved in the 2-DoF over-constrained PM, the $\hat{\$}_{\mathrm{ta},j,i}$ can be expressed in axis-coordinate as

$$\hat{\$}_{\mathrm{ta},j,i} = \left(\boldsymbol{r}_{j,i} \times \boldsymbol{s}_{j,i}, \boldsymbol{s}_{j,i}\right)^{\mathrm{T}} \tag{2}$$

herein $s_{j,i}$ is the vector of the rotational axis of jth joint and $r_{j,i}$ is the vector pointing from point C_E to any point on the axis.

Reciprocal screw product is defined as the instantaneous work contributed by the wrench during the motion along the twist [23]. If a wrench does not do work on a twist, their reciprocal product is zero. The wrench and twist are then described as reciprocal. Therefore, the constrained wrench of the limb is the reciprocal screw of all the joint twists, which is derived by computing the six-dimensional vector having zero inner products with all the joint twists. The constrained wrenches of RSR limbs and SS limb are derived as

$$\hat{\$}_{\mathrm{wc},i} = \begin{pmatrix} \boldsymbol{s}_{c,i} \\ \boldsymbol{C}_E\boldsymbol{S}_i \times \boldsymbol{s}_{c,i} \end{pmatrix}, \quad \hat{\$}_{\mathrm{wc},5} = \begin{pmatrix} \boldsymbol{r}/h \\ \boldsymbol{0}_{1\times 3} \end{pmatrix} \tag{3}$$

where $\boldsymbol{C}_E\boldsymbol{S}_i$ are the vectors from point C_E to point S_i. $\boldsymbol{s}_{c,i}$ is the intersection line of two planes formed by R joints and links, i.e. the first R joint and RS link, the fifth R joint and SR link. $\boldsymbol{s}_{c,i} = \boldsymbol{l}_{1,i} \times \boldsymbol{l}_{2,i}$, $\boldsymbol{l}_{1,i} = \boldsymbol{s}_{5,i} \times \boldsymbol{S}_i\boldsymbol{A}_i$, $\boldsymbol{l}_{2,i} = \boldsymbol{s}_{1,i} \times \boldsymbol{S}_i\boldsymbol{B}_i$, $i = 1, 2, 3, 4$. $\boldsymbol{r}$ is the vector from point O to point C_E.

Mobility of the PM can be analyzed by the constraints of the mechanism, which is to find out the independent constrained forces and toruques. Due to the symmetrical structure, $\boldsymbol{s}_{c,i}$ $(i = 1, 2, 3, 4)$ is located on the plane formed by the centers of the S joints, indicating that the constrained wrenches of the RSR limbs are all on this plane. These constrained wrenches are constrained forces that opposite ones are parallel and adjacent ones are perpendicular ($\boldsymbol{s}_{\mathrm{c},1} // \boldsymbol{s}_{\mathrm{c},3}, \boldsymbol{s}_{\mathrm{c},2} // \boldsymbol{s}_{\mathrm{c},4}, \boldsymbol{s}_{\mathrm{c},1} \perp \boldsymbol{s}_{\mathrm{c},2}, \boldsymbol{s}_{\mathrm{c},3} \perp \boldsymbol{s}_{\mathrm{c},4}$). According to geometry, a plane is uniquely determined by arbitrary two lines. Hence, two independent constrained forces on the plane and the constrained force of SS limb constitute the full space of forces. In other words, there exists redundant force on the plane since there are at most three linear independent forces for any rigid body. For the constrained torques, it is found that an equivalent torque about the normal direction of the plane is formed by the opposite constrained forces. Altogether, the constraints of the mechanism are three independent forces and one torque. Based on the dual relations between motions and constraints, the mobility of the mechanism is two rotations. There are only four linear independent wrenches provided by limbs, resulting in one extra constrained wrench to the moving platform. Hence, this PM is over-constrained.

To achieve large rotating capability, S joints of the physical prototype are replaced by three perpendicular R joints during fabrication. The moving platform of the 2-DoF over-constrained PM can rotate within the range $\pm 90°$. TwinCAT NC PTP developed by Beckhoff Automation [24] is applied to the motion control. Comparing with the conventional motion controllers, TwinCAT NC PTP works on the same CPU as PLC, contributing to a fast and direct data exchange between the motion and logic controller. The motion control block is shown in Fig. 2. It is divided into three phases, i.e. PLC, NC and physical axes. PLC phase contains motion and IO control program. The IO control program can directly control the IO devices such as indicator lights and sensors. Motion control program is based on the kinematic model of the 2-DoF over-constrained PM. The desired motion of end-effector (including displacement, velocity and acceleration) is derived by controlling the output of motors. Control order is sent to the NC motion controller and then to the motor drives.

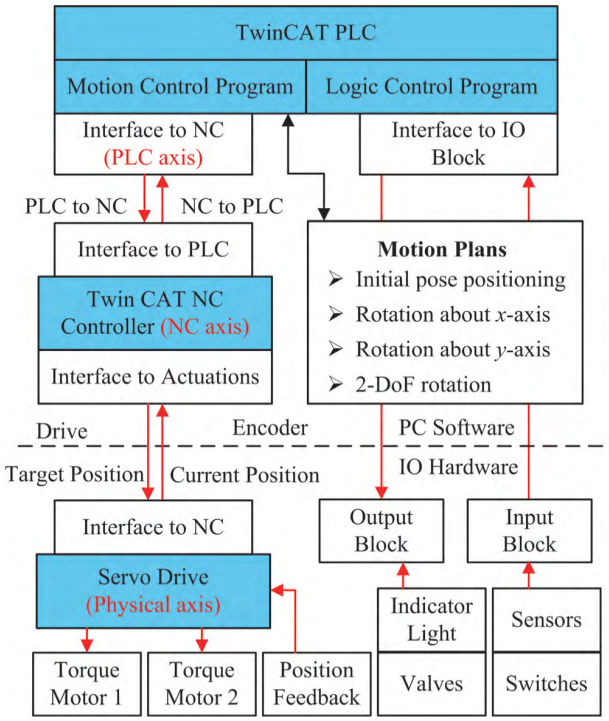

FIGURE 2. Motion control block of the 2-DoF over-constrained PM.

Motion inaccuracy is compensated by both modifying motor outputs according to the kinematic calibration results and motion information of the moving platform obtained from the feedback control.

III. GEOMETRIC ERROR MODELING BY REAL INVERSE KINEMATICS

The inverse position analysis without geometric errors is firstly carried out by closed-loop vector equations. Tilt-Torsion angles [6] are applied to describe the pose of the moving platform. The rotation matrix of the frame $C_E - uvw$ with respect to the frame $O - xyz$ is expressed as

$$\boldsymbol{R} = \begin{bmatrix} c^2\phi c\theta + s^2\phi & s\phi c\phi c\theta - s\phi c\phi & c\phi s\theta \\ s\phi c\phi c\theta - s\phi c\phi & s^2\phi c\theta + c^2\phi & s\phi s\theta \\ -c\phi s\theta & -s\phi s\theta & c\theta \end{bmatrix} \quad (4)$$

where s and c denote sine and cosine. ϕ, θ are azimuth, tilt angles, $\phi \in [0,\ 2\pi]$, $\theta \in [0,\ \pi]$.

The closed-loop vector equations are formulated as

$$\boldsymbol{b}_j + l\boldsymbol{w}_{1,j} + l\boldsymbol{w}_{2,j} = \boldsymbol{r} + \boldsymbol{R}\boldsymbol{a}_j, \quad j = 1, 2 \quad (5)$$

where $\boldsymbol{b}_j$ is the vector of point B_i in the frame $O - xyz$. $\boldsymbol{w}_{1,j}$, $\boldsymbol{w}_{2,j}$ are the unit vectors of $\overrightarrow{B_jS_j}$ and $\overrightarrow{S_jA_j}$. $\boldsymbol{w}_{1,1} = \boldsymbol{R}_{y,\beta_1}\boldsymbol{e}_1$, $\boldsymbol{w}_{1,2} = \boldsymbol{R}_{z,\pi/2}\boldsymbol{R}_{y,\beta_2}\boldsymbol{e}_1$. Herein, $\boldsymbol{R}_{z,\pi/2}$ is the orientation matrix that rotates about z-axis with $\pi/2$. $\boldsymbol{R}_{y,\beta_1}, \boldsymbol{R}_{y,\beta_2}$ are the rotation matrices about y-axis with β_1 and β_2. $\boldsymbol{e}_1 = \begin{pmatrix} 1 & 0 & 0 \end{pmatrix}^{\mathrm{T}}$. $\boldsymbol{r}$ is position vector of point C_E. $\boldsymbol{a}_j$ is the vector of point A_i in frame $C_E - uvw$. And

$$\boldsymbol{b}_1 = \boldsymbol{a}_1 = \begin{pmatrix} a & 0 & 0 \end{pmatrix}^{\mathrm{T}}, \quad \boldsymbol{b}_2 = \boldsymbol{a}_2 = \begin{pmatrix} 0 & a & 0 \end{pmatrix}^{\mathrm{T}}$$

TABLE 1. Geometric errors of RSR limb.

Errors	Definition
${}^0\delta x_{1,j}$, ${}^0\delta y_{1,j}$, ${}^0\delta z_{1,j}$	Position errors of point B_j respect to fixed frame
${}^0\delta\alpha_{1,j}$, ${}^0\delta\gamma_{1,j}$	Orientation errors of 1st R joint
${}^1\delta x_{2,j}$, ${}^1\delta y_{2,j}$	Position errors of point S_j respect to 1st R joint
${}^4\delta x_{5,j}$, ${}^4\delta z_{5,j}$	Position errors of point A_j respect ot point S_j
${}^6\delta x_{5,j}$, ${}^6\delta z_{5,j}$	Position errors of point A_j respect to moving frame

The closed-loop equations are further organized as

$$\left\| \boldsymbol{r} + \boldsymbol{R}\boldsymbol{a}_j - \boldsymbol{b}_j - l\boldsymbol{w}_{1,j} \right\| = l \quad (6)$$

The position vector of point C_E can be obtained through

$$\boldsymbol{r} = \begin{pmatrix} hc\phi s\dfrac{\theta}{2} & hs\phi s\dfrac{\theta}{2} & hc\dfrac{\theta}{2} \end{pmatrix}^{\mathrm{T}} \quad (7)$$

Hence, the input angles β_1 and β_2 can be computed via (6) and (7) when the orientation angles ϕ, θ are given.

By adding geometric errors, the closed-loop vector equations for real inverse position analysis are re-formulated. The vectors expressed by nominal parameters in (5) will be replaced by the actual parameters that contain position or orientation errors of joints.

The $\boldsymbol{b}_j$ becomes $\boldsymbol{b}_j + \Delta\boldsymbol{b}_j$ because of position errors of point B_i. Herein, $\Delta\boldsymbol{b}_j$ is defined as

$$\Delta\boldsymbol{b}_j = \begin{pmatrix} {}^0\delta x_{1,j} & {}^0\delta y_{1,j} & {}^0\delta z_{1,j} \end{pmatrix}^{\mathrm{T}} \quad (8)$$

The $l\boldsymbol{w}_{1,j}$ turns into $(l + \Delta l_{1,j})\boldsymbol{w}'_1$ due to the error of link length and the orientation error of link $\overrightarrow{B_jS_j}$. This orientation error is led by the orientation errors of R joint connecting to the fixed base. $\boldsymbol{w}'_1$ is defined as

$$\boldsymbol{w}'_1 = \boldsymbol{w}_1 + \Delta\boldsymbol{w}_1 \times \boldsymbol{w}_1 \quad (9)$$

where $\Delta\boldsymbol{w}_1 = \begin{bmatrix} 0 & -{}^0\delta\gamma_{1,1} & 0 \\ {}^0\delta\gamma_{1,1} & 0 & -{}^0\delta\alpha_{1,1} \\ 0 & {}^0\delta\alpha_{1,1} & 0 \end{bmatrix}$. ${}^0\delta\alpha_{1,1}$, ${}^0\delta\gamma_{1,1}$ are the orientation errors along the local frame $B_j - x_jy_jz_j$, in which y_i-axis is collinear with the rotation axis of R joint.

The actual expression of $l\boldsymbol{w}_{2,j}$ is formulated in the same way as $l\boldsymbol{w}_{1,j}$. Similarly, $\boldsymbol{a}_j$ becomes $\boldsymbol{a}'_j + \Delta\boldsymbol{a}_j$, and

$$\boldsymbol{a}'_1 = \begin{pmatrix} a & 0 & -h_s \end{pmatrix}^{\mathrm{T}}, \quad \boldsymbol{a}'_2 = \begin{pmatrix} 0 & a & -h_s \end{pmatrix}^{\mathrm{T}} \quad (10)$$

$$\Delta\boldsymbol{a}_j = \begin{pmatrix} {}^6\delta x_{5,j} & {}^6\delta y_{5,j} & {}^6\delta z_{5,j} \end{pmatrix}^{\mathrm{T}} \quad (11)$$

where h_s is the distance from the upper surface of moving platform to the point A_j. ${}^6\delta x_{5,j}$, ${}^6\delta y_{5,j}$ and ${}^6\delta z_{5,j}$ are the position errors of point A_j in the frame $C_E - uvw$.

The geometric errors of each RSR limb is summarized in Table 1, where

$$\begin{aligned} {}^1\delta x_{2,j} &= \Delta l_{1,j}\sin(\theta_{\mathrm{L}}), \quad {}^1\delta y_{2,i} = -\Delta l_{1,i}\cos(\theta_{\mathrm{L}}), \\ {}^4\delta x_{5,j} &= \Delta l_{2,j}\sin(\theta_{\mathrm{H}}), \quad {}^4\delta z_{5,j} = \Delta l_{2,j}\cos(\theta_{\mathrm{H}}). \end{aligned}$$

With the real parameters, the real inverse position model can be formulated as

$$\boldsymbol{b}_j + \Delta\boldsymbol{b}_j + (l + \Delta l_{1,j})\boldsymbol{w}'_1 + (l + \Delta l_{2,j})\boldsymbol{w}'_1 = \boldsymbol{r}' + \boldsymbol{R}(\boldsymbol{a}_j + \Delta\boldsymbol{a}_j) \quad (12)$$

where $\boldsymbol{r}'$ is the measured position vector of point C_E. There is no errors in $\boldsymbol{R}$ because the axes of established fixed and moving frames are assumed to be correct references, which will be explained in Section V.

The actual inputs of the 2-DoF over-constrained PM are computed by solving (12).

$$\beta_j = 2\arctan\left(\left(-B_j + \sqrt{B_j^2 - C_j^2 + A_j^2}\right)/\left(C_j - A_j\right)\right) \quad (13)$$

The computation of A_j, B_j and C_j are shown in Appendix. The geometric errors in the presented study are defined in the same way as the previous error modeling methods. The difference lies in the way of formulating error models. In the conventional methods, the displacement equations of PMs are differentiated to obtain the mapping error model. In our method, however, geometric errors are directly added to the inverse position analysis. Coupling items between the geometric errors appear when calculating the mechanism inputs. As a result, the nonlinear geometric error models are formulated.

IV. PARAMETER IDENTIFICATION BY HGA

After the geometric error model is built, measurement planning and parameter identification are implemented. Herein, Laser tracker is selected as the measuring device. With the measuring poses of the moving platform, the identification equations are formulated as

$$f_s = \sum_{s=1}^{N} \left(\beta_{j,s} - \beta_{j,s,0} - \Delta\theta_{j,s,0}\right)^2 \quad (14)$$

where $\beta_{j,s}$, $\beta_{j,s,0}$ are the actual and nominal inputs of the jth RSR limb, $\Delta\theta_{j,s,0}$ is the home position error. Herein, the geometric errors are unknown variables incorporating with the measuring poses on the right side of the equations. There are two closed-loops, thus two identification equations are formulated.

For the inverse position analysis of PMs, certain inputs can be analytically computed under any configurations selected from nonsingular workspace. Due to this feature, random measuring configurations can be selected for solving identification equations shown in (14). To achieve the best compromise between efficiency and accuracy, measuring points should be 2∼3 times more than the numbers of geometric errors [10]. There are 11 geometric errors in each limb, thus 24 evenly distributed measuring points are finally selected. Herein, any number that is between 22 and 33 points are acceptable.

In terms of solving nonlinear equations, nonlinear optimization method is adopted. The identification equation is turned into an objective function and the optimization problem can be described as: finding out the optimal geometric errors that make f_s be minimal. Since unique mechanism inputs can be obtained when giving certain poses of moving platform, $\min f_s = 0$ exists and the optimal parameters are just the desired geometric errors.

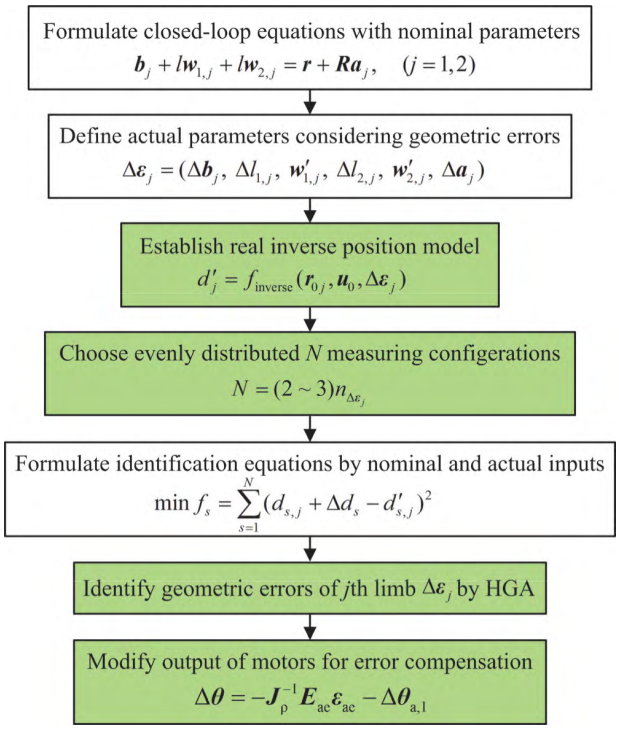

FIGURE 3. Kinematic calibration procedure of the 2-DoF over-constrained PM.

Mathematically, the optimization for determining geometric errors is a nonlinear convex programming problem without constraints. There have been local and global searching methods to deal with this problem. Local searching algorithms such as sequential quadratic programming (SQP) [26] have rapid local convergence. But the results are dependent on the initial starting point whose selection is difficult, and they would stop searching if a local optimum is obtained. Genetic algorithm (GA), as one of the most important global searching methods, is robust and insensitive to initial point. However, GA has difficulties in the convergence rate of a local search. It spends most of the time competing between different hills, rather than improving solutions on single hill where optimal point is located [27].

By combining SQP and GA, a HGA method has been proposed [28], [29]. The implementation is divided into two phases. In the first phase, GA is employed to provide the potential near optimum solution. By regarding it as starting point, SQP is applied to search for the precise optimum with high speed in the second phase. Taking the advantage of GA and SQP, the HGA is improved effectively and efficiently.

After parameter identification by HGA, modifications of motor outputs in controller are employed to compensate geometric errors as

$$\Delta\boldsymbol{\theta} = -\boldsymbol{J}_\rho^{-1}\boldsymbol{E}_{\text{ae}}\boldsymbol{\varepsilon}_{\text{ae}} - \Delta\boldsymbol{\theta}_{\text{a,1}} \quad (15)$$

where $\boldsymbol{J}_\rho$ is Jacobian matrix computed by nominal velocity analysis [6]. $\Delta\boldsymbol{\theta}_{\text{a,1}}$ and $\boldsymbol{\varepsilon}_{\text{ae}}$ are output errors of motors and geometric errors. $\boldsymbol{E}_{\text{ae}}$ is the error coefficient matrix.

The procedure of the kinematic calibration method by the real inverse kinematic and HGA is summarized in Fig. 3.

V. SIMULATION AND EXPERIMENT

Through inserting given values of geometric errors to the ideal prototype, calibration simulation is firstly carried out by SolidWorks software. The identified errors are then compared with the initial given values to verify the effectiveness of proposed method.

The nominal parameters of the 2-DoF over-constrained PM, i.e. a, h, l and h_s are given by 150, 402, 317 and 80 mm. Then 24 measuring points are evenly chosen from the workspace. The simulation is implemented as follow.

(1) Draw 3D sketch of the 2-DoF over-constrained PM in SolidWorks. Establish the fixed frame O-xyz according to the schematic diagram and insert the given geometric errors.

(2) Drive the 3D sketch model to the 24 measuring points. Select nonlinear points P_1, P_2, P_3 on the moving platform. Measure their coordinates at each measuring configuration. In order to consider measuring noise from laser tracker, white noise with mean value 0, standard deviation 0.01mm is applied to the coordinates of measuring points.

(3) Compute the rotation matrix $\boldsymbol{R} = \begin{bmatrix} \boldsymbol{u} & \boldsymbol{v} & \boldsymbol{w} \end{bmatrix}$ by

$$\begin{cases} \boldsymbol{u} = \left(\overrightarrow{P_2P_1}\right) \Big/ \left\| \left(\overrightarrow{P_2P_1}\right) \right\| \\ \boldsymbol{w} = \left(\overrightarrow{P_2P_1} \times \overrightarrow{P_2P_3}\right) \Big/ \left\| \left(\overrightarrow{P_2P_1} \times \overrightarrow{P_2P_3}\right) \right\| \\ \boldsymbol{v} = \boldsymbol{w} \times \boldsymbol{u} \end{cases} \tag{16}$$

(4) Formulate parameter identification equations by the measuring configurations. Perform programing in Matlab.

(5) Apply HGA by Matlab Genetic Algorithm Toolbox. In the settings, the population size is given as 100. The optimization generations are 3000. The elite generations are 8. The probability of crossover and mutation probability are assigned as 0.7 and 0.1. The *fmincon* and SQP are selected as the solver and hybrid algorithm. The stopping criteria are set as TolX=10^{12}, TolFun=10^{100}.

Comparisons between the predefined and identified geometric errors are shown in Table 2. The maximum deviation of the position error is 0.399 mm while the maximum deviation of the orientation error is 0.03°. In the whole, the average deviation is 9.52%, which confirms the effectiveness of the calibration method.

TABLE 2. Predefined and identified geometric errors by simulation (unit for position errors are mm and orientation errors are deg).

No.	Error	Predefined	Identified	No.	Error	Predefined	Identified
1	${}^0\delta x_{1,1}$	-1.5	-1.488	12	${}^0\delta x_{1,2}$	-1	-1.16
2	${}^0\delta y_{1,1}$	1.3	1.275	13	${}^0\delta y_{1,2}$	-0.45	-0.416
3	${}^0\delta z_{1,1}$	-1	-1.096	14	${}^0\delta z_{1,2}$	-1.5	-1.489
4	${}^0\delta \alpha_{1,1}$	0	0	15	${}^0\delta \alpha_{12}$	0.2	0.23
5	${}^0\delta \gamma_{1,1}$	-0.1	-0.11	16	${}^0\delta \gamma_{1,2}$	0.2	0.17
6	$\Delta l_{1,1}$	0.382	0.213	17	$\Delta l_{1,2}$	-0.4	-0.377
7	$\Delta l_{2,1}$	1.214	1.107	18	$\Delta l_{2,2}$	0.5	0.488
8	${}^6\delta x_{5,1}$	1.4	1.349	19	${}^6\delta x_{5,2}$	1.5	1.449
9	${}^6\delta y_{5,1}$	1.3	0.901	20	${}^6\delta y_{5,2}$	2	1.986
10	${}^6\delta z_{5,1}$	1.2	1.119	21	${}^6\delta z_{5,2}$	0.3	0.27
11	$\Delta\theta_{a,1}$	-0.28	-0.305	22	$\Delta\theta_{a,2}$	-0.4	-0.37

Simulation results also indicate that the random selected measurement configurations lead to high accuracy. The same set of measurement points can be applied for the parameter identification of different limbs. The efficiency of the whole calibration process is greatly improved.

Kinematic calibration experiments are also implemented. The experimental setup is as shown in Fig. 4. First of all, the fixed and moving frames are established. The fixed frame is assigned according to the datum holes on the fixed base. The center of these datum holes are defined as point Q_1, Q_2, Q_3 and Q_4. The line going through point Q_1 and Q_3 is set as x-axis. The normal direction of the plane formed by point Q_1, Q_2, Q_3 and Q_4 is collinear with z-axis. The y-axis is determined by default. Since the laser tracker is capable of finding the center of S joint, the origin of fixed base can be accurately found out. Hence, the frame $O-xyz$ is successfully set up. Similarly, the non-collinear points Q_5, Q_6, Q_7 and Q_8 are selected from the moving platform.

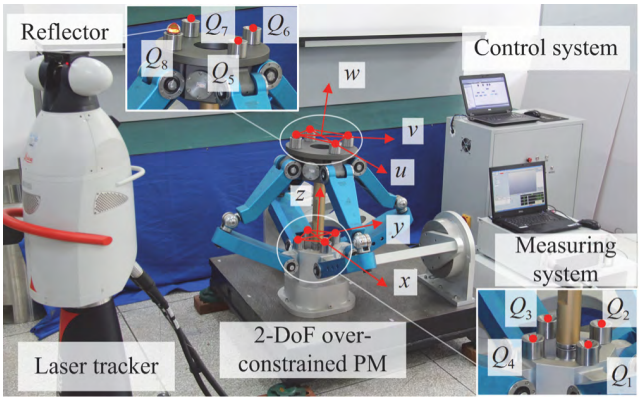

FIGURE 4. Kinematic calibration experimental setup.

Herein, the u-axis is defined by point Q_5 and Q_7 while the w-axis is determined by the plane formed by all the four points. From this procedure, it is noted that both the fixed and moving frames are established through the references on the fixed base and moving platform. Geometric errors of parts are expressed as the relative errors to these frames. In other words, the axes of established frames are regarded as corrected references. On this basis, the geometric errors are defined. The position errors of point O and $\boldsymbol{C}_{\mathrm{E}}$ are considered by the home position error $\Delta\theta_{j,s,0}$ and the position vector $\boldsymbol{r}'$. Hence, the rotation matrix $\boldsymbol{R}$ is assumed to be without errors in the error modeling process.

With the same manner as simulation, the orientation matrix can be computed by (16). The orientation angles are obtained as

$$\theta = \arccos(R_{33}), \quad \phi = \arctan\left(\frac{R_{23}}{R_{13}}\right) \tag{17}$$

where R_{13}, R_{23} and R_{33} are the elements in the third column of the orientation matrix $\boldsymbol{R}$.

Then, the identification equations can be formulated with the measuring data obtained from all measuring points

according to (14). Herein, the measuring points are the same as the points adopted in simulation. The HGA is applied to identify the geometric errors. Finally, error compensation is implemented through modifying the motor outputs by (15). To evaluate error compensation results, the calibrated 2-DoF over-constrained PM would be driven towards 24 testing points, as shown in Fig. 5. It is found that the orientation angles largely deviate from the expected values before calibration. For all testing points, the average deviations of θ and φ are 0.3069° and 1.3586°. The maximum deviation of both angles are up to 0.4632° and 3.205°. After calibration by the proposed method, the maximum deviation of θ drops to 0.0249°, and the average is reduced to 0.0059°. The maximum and average differences of φ become 0.1452° and 0.0337°. In general, the accuracy improvements for θ and φ are 93.96% and 90.38%, this proves the high accuracy of the proposed kinematic calibration method for over-constrained PMs.

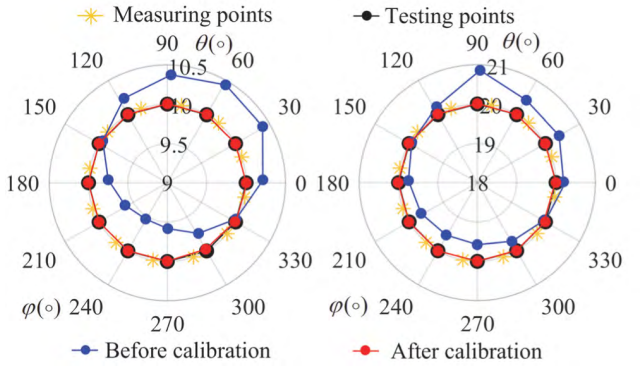

FIGURE 5. Orientation angles of testing points before and after calibration.

VI. DISCUSSION

In the presented calibration method, error model by the real inverse position analysis and the parameter identification by HGA are essential. In order to further discuss feasibility of this method, comparative studies on these two steps are carried out in this section.

A. KINEMATIC CALIBRATION BASED ON REGULARIZATION METHOD

For the 2-DoF over-constrained PM, the direct error mapping model is as follow [30].

$$\$_{\mathrm{t}} = \boldsymbol{J}_{\mathrm{e}}\boldsymbol{\varepsilon}_{\mathrm{e}} \tag{18}$$

where $\boldsymbol{J}_{\mathrm{e}} = \left(\boldsymbol{J}_{\mathrm{x}}^{\mathrm{T}}\boldsymbol{J}_{\mathrm{x}}\right)^{-1}\boldsymbol{J}_{\mathrm{x}}^{\mathrm{T}}\boldsymbol{E}_{\mathrm{e}}$ is error Jacobian matrix. $\boldsymbol{J}_{\mathrm{x}}$ is formed by all actuation and constrained wrenches, $\boldsymbol{E}_{\mathrm{e}}$ is coefficient matrix corresponding to geometric errors of all limbs. The same 22 geometric errors are included in this geometric error mapping model.

96 evenly distributed measuring poses are selected from the orientation workspace. The laser tracker is adopted again for measuring position of points on the moving platform, from which the orientation angles are computed. By incorporating the measuring data, the error model becomes

$$\Delta\boldsymbol{X}_p = \boldsymbol{H}\Delta\boldsymbol{\varepsilon} \tag{19}$$

where $\Delta\boldsymbol{X}_p$ denotes the pose errors of the moving platform under 96 measuring poses. $\boldsymbol{H}$ is identification matrix consisting of error Jacobian matrices under 96 measuring poses.

For the 2-DoF over-constrained PM, the condition number of $\boldsymbol{H}$ is 6.72×10^4. The accuracy of the calculated geometric errors is low if the inverse of $\boldsymbol{H}$ is directly applied. To solve this problem, a regularization parameter λ is applied to control quality of the solutions.

In order to find a suitable λ, the parametric plot of $x(\lambda)$ and $y(\lambda)$ is investigated. Herein, $x(\lambda) = \left\|\Delta\boldsymbol{X}_p - \boldsymbol{H}\Delta\boldsymbol{\varepsilon}\right\|$ and $y(\lambda) = \|\Delta\boldsymbol{\varepsilon}\|$ for all $\lambda > 0$. The corner of the obtained curve shows a good balance between the regularization error $y(\lambda)$ and the right-hand error $x(\lambda)$ [14]. Corresponding λ is chosen as the regularization parameter. The identification equations can be formulated with the determined λ as

$$\Delta\boldsymbol{\varepsilon} = \left(\boldsymbol{H}^{\mathrm{T}}\boldsymbol{H} + \lambda\boldsymbol{I}\right)^{-1}\boldsymbol{H}^{\mathrm{T}}\Delta\boldsymbol{X}_p \tag{20}$$

Kinematic calibration experiment based on regularization method is carried out. The deviations of orientation angles at testing points are shown in Fig. 6. The maximum deviation of θ and φ at testing points after calibration by regularization method are 0.4706° and 0.4682°, and the average deviations are 0.247° and 0.352°. Comparing with our method, the orientation deviations for both angles are larger. Accuracy improvement of θ and φ are 5.815% and 74.189% by regularization method. It indicates that our method has better accuracy than the regularization method. Besides, measuring points of our method are less. The whole calibration process is more efficient.

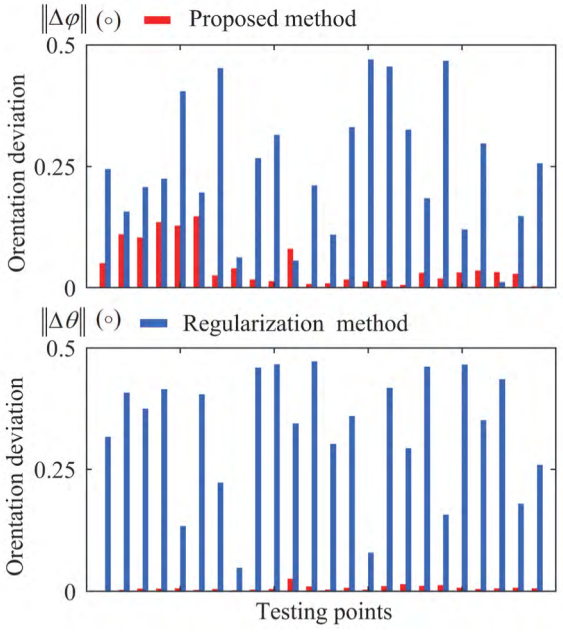

FIGURE 6. Deviation of orientation angles by two calibration methods.

B. OPTIMIZATION ALGORITHMS FOR NONLINEAR PARAMETER IDENTIFICATION

Since the nonlinear error model is built by inverse position analysis of the 2-DoF over-constrained PM, the nonlinear identification equations can always find a set of geometric errors that make the deviations of the real and nominal motor outputs are minimal. Therefore, the parameter identification can be achieved by optimization algorithm.

Besides HGA, four commonly used optimization algorithms for non-linear problems are applied, i.e. genetic algorithm (GA), Levernberg Marquadt (LM), Simulated Annealing (SA) and Particle Swarm Optimization (PSO).

1) GA

GA is based on biological evolution that repeatedly modifies a population of individual solutions. At each step, GA selects individuals to be parents randomly from the current population. Two parents are combined to form children for the next generation by crossover and mutation. The population moves toward optimal solution over successive generations.

2) LM

LM is a damped least-square method arising from least squares curve fitting. LM interpolates between the Gauss-Newton algorithm and gradient descent method. The choice of damping parameter depends on the initial searching point.

3) SA

SA is a probabilistic technique that approximates the global optimum. SA randomly generated a new point at each iteration. The searching distance of the new point from the current point is set by a probability distribution. By accepting the points that raise the objective, SA is able to explore globally for better solutions.

4) PSO

PSO is inspired by the social behavior like bird flock or fish school. PSO solves a problem through a population with candidate solutions, called particles. It moves these particles in the searching space according to the position and velocity of the particle. Each particle's movement is influenced by its local best known position, but is also guided toward the best known positions of its neighbors.

The same set of predefined geometric errors as Section V is chosen. Through simulation, deviations between the predefined and the identified errors by different optimization algorithms are shown in Fig. 7 and Fig. 8. In general, position errors identified by SA have the worst accuracy. For instance, the identified ${}^{6}\delta z_{5,1}$ is -1.707 mm when it is given as 1.2 mm. The maximum deviation is up to 2.907 mm. The accuracy of LM is also unacceptable. The identified ${}^{0}\delta x_{1,1}$ is -0.102 mm when the predefined value is -1.5 mm. For the GA, the maximum deviation is 1.706 mm. If the generation of PSO is set as 30,000, the identified errors of the 1st RSR

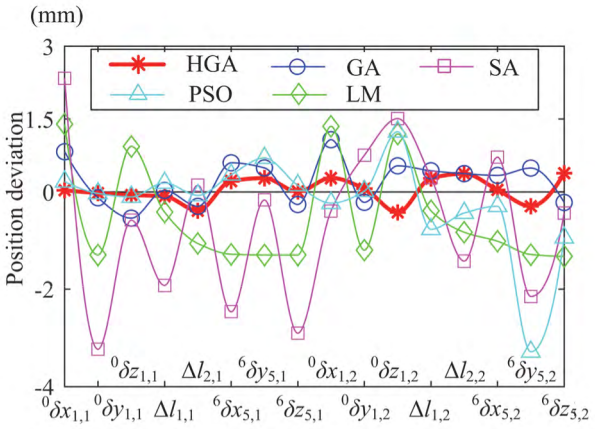

FIGURE 7. Deviation of position errors by different optimization algorithms.

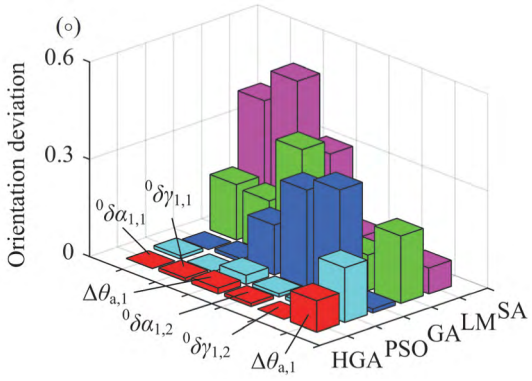

FIGURE 8. Deviation of orientation errors by different optimization algorithms.

limb has better consistency with the predefined errors than the 2nd RSR limb. The maximum deviation is -3.29 mm in ${}^{6}\delta y_{5,2}$. Comparatively, the maximum deviation of the position errors by HGA is the smallest (-0.385 mm). Similar results are obtained for the orientation errors. The ranking of the maximum deviations is SA (0.5°), LM (0.357°), GA (0.34°), PSO (0.169°) and HGA (0.096°). In the whole, the identified position errors by HGA stay close to the predefined errors. It confirms the high accuracy of HGA.

VII. CONCLUSION

This paper deals with the kinematic calibration of a 2-DoF over-constrained PM. By inserting geometric errors of the parts to the inverse position analysis, the geometric error model is firstly built. It is divided into two sub-models according to the closed-loop equations. These sub-models allow separate parameter identification of limbs with the same set of measuring poses, thereby increasing efficiency of calibration process.

Nonlinear identification equations are then formulated by randomly selected measuring poses. They are turned into nonlinear optimization problem and then HGA is applied.

HGA combines the global convergence of GA and the fast searching capability of SQP, hence can search for the geometric errors in an efficient and accurate manner. Finally, error compensation is implemented by modifying the motor outputs.

The proposed method is testified by simulation and experiments. The results show that orientation accuracy improvements of the 2-DoF over-constrained PM are up to 93.96% and 90.38%. Comparatively, Kinematic calibration based on the regularization method improves accuracy by 5.815% and 74.819%. Different optimization algorithms, including GA, LM, SA and PSO, are further compared with the HGA in parameter identification. The comparisons indicate that the error modeling by real inverse kinematics and the parameter identification by HGA contribute to the high accuracy of the proposed calibration method. The presented work lays a solid foundation for the following motion control of the 2-DoF over-constrained PM. It can also be applied to the kinematic calibration of any PM.

APPENDIX

The coefficients of (13) are as follow.

$$
\begin{aligned}
A_1 &= 2\lambda_{1,1}(l+\Delta l_{1,1})\cos({}^0\delta\gamma_{1,1}) + 2\lambda_{2,1}(l+\Delta l_{1,1}) \\
&\quad \times \cos({}^0\delta\alpha_{1,1})\sin({}^0\delta\gamma_{1,1}) + 2\lambda_{3,1}(l+\Delta l_{1,1}) \\
&\quad \times \sin({}^0\delta\alpha_{1,1})\sin({}^0\delta\gamma_{1,1}), \\
B_1 &= 2\lambda_{2,1}(l+\Delta l_{1,1})\sin({}^0\delta\alpha_{1,1}) - 2\lambda_{3,1}(l+\Delta l_{1,1}) \\
&\quad \times \cos({}^0\delta\alpha_{1,1}), \\
C_1 &= (l+\Delta l_{1,1})^2 + \lambda_{1,1}^2 + \lambda_{2,1}^2 + \lambda_{3,1}^2 - (l+\Delta l_{2,1})^2, \\
A_2 &= -2\lambda_{1,2}(l+\Delta l_{1,2})\cos({}^0\delta\alpha_{1,2})\sin({}^0\delta\gamma_{1,2}) \\
&\quad + 2\lambda_{2,2}(l+\Delta l_{1,2})\cos({}^0\delta\gamma_{1,2}) + 2\lambda_{3,2}(l+\Delta l_{1,2}) \\
&\quad \times \sin({}^0\delta\alpha_{1,2})\sin({}^0\delta\gamma_{1,2}), \\
B_2 &= -2\lambda_{1,2}(l+\Delta l_{1,2})\sin({}^0\delta\alpha_{1,2}) \\
&\quad - 2\lambda_{3,2}(l+\Delta l_{1,2})\cos({}^0\delta\alpha_{1,2}), \\
C_2 &= (l+\Delta l_{1,2})^2 + \lambda_{1,2}^2 + \lambda_{2,2}^2 + \lambda_{3,2}^2 - (l+\Delta l_{2,2})^2, \\
\lambda_{1,1} &= a + {}^0\delta x_{1,1} - r_x - \boldsymbol{R}_1(\boldsymbol{a}_1 + \Delta\boldsymbol{a}_1), \\
\lambda_{2,1} &= {}^0\delta y_{1,1} - r_y - \boldsymbol{R}_2(\boldsymbol{a}_1 + \Delta\boldsymbol{a}_1), \\
\lambda_{3,1} &= {}^0\delta z_{1,1} - r_z - \boldsymbol{R}_3(\boldsymbol{a}_{10} + \Delta\boldsymbol{a}_{10}), \\
\lambda_{1,2} &= -{}^0\delta y_{1,2} - r_x - \boldsymbol{R}_1\left(\boldsymbol{a}_2 + \boldsymbol{R}_{z,\pi/2}\Delta\boldsymbol{a}_2\right), \\
\lambda_{2,2} &= a + {}^0\delta x_{1,2} - r_y - \boldsymbol{R}_2\left(\boldsymbol{a}_2 + \boldsymbol{R}_{z,\pi/2}\Delta\boldsymbol{a}_2\right), \\
\lambda_{3,2} &= {}^0\delta z_{1,2} - r_z - \boldsymbol{R}_3\left(\boldsymbol{a}_2 + \boldsymbol{R}_{z,\pi/2}\Delta\boldsymbol{a}_2\right).
\end{aligned}
$$

Herein, $\boldsymbol{r} = (r_x\ r_y\ r_z)^{\mathrm{T}}$, $\boldsymbol{R}_k$ $(k = 1, 2, 3)$ is the kth row of orientation matrix $\boldsymbol{R}$.

REFERENCES

[1] T. Huang, D. G. Chetwynd, J. P. Mei, and X. M. Zhao, "Tolerance design of a 2-DOF overconstrained translational parallel robot," *IEEE Trans. Robot.*, vol. 22, no. 1, pp. 167–172, Feb. 2006.

[2] A. Pashkevich, D. Chablat, and P. Wenger, "Stiffness analysis of 3-d.o.f. overconstrained translational parallel manipulators," in *Proc. IEEE Int. Conf. Robot. Automat.*, Pasadena, CA, USA, May 2008, pp. 1562–1567.

[3] O. Linda and M. Manic, "Uncertainty-robust design of interval type-2 fuzzy logic controller for delta parallel robot," *IEEE Trans. Ind. Informat.*, vol. 7, no. 4, pp. 661–670, Nov. 2011.

[4] Y. Jiang, T. Li, L. Wang, and F. Chen, "Kinematic accuracy improvement of a novel smart structure-based parallel kinematic machine," *ASME/IEEE Trans. Mechatron.*, vol. 23, no. 1, pp. 469–481, Feb. 2018.

[5] B. Li, Y. Li, and X. Zhao, "Kinematics analysis of a novel over-constrained three degree-of-freedom spatial parallel manipulator," *Mech. Mach. Theory*, vol. 104, pp. 222–233, Oct. 2016.

[6] Y. Qi, T. Sun, and Y. Song, "Multi-objective optimization of parallel tracking mechanism considering parameter uncertainty," *J. Mech. Robot.*, vol. 10, pp. 041006-1–041006-12, Aug. 2018.

[7] M. Sharifzadeh, M. T. Masouleh, A. Kalhor, and P. Shahverdi, "An experimental dynamic identification & control of an overconstrained 3-DOF parallel mechanism in presence of variable friction and feedback delay," *Robot. Auton. Syst.*, vol. 102, pp. 27–43, Apr. 2018.

[8] D. Zhang and Z. Gao, "Optimal kinematic calibration of parallel manipulators with pseudoerror theory and cooperative coevolutionary network," *IEEE Trans. Ind. Electron.*, vol. 59, no. 8, pp. 3221–3231, Aug. 2012.

[9] Y. Wu, A. Klimchik, S. Caro, B. Furet, and A. Pashkevich, "Geometric calibration of industrial robots using enhanced partial pose measurements and design of experiments," *Robot. Comput. Integr. Manuf.*, vol. 35, pp. 151–168, Oct. 2015.

[10] J. Wang and O. Masory, "On the accuracy of a stewart platform. I. The effect of manufacturing tolerances," in *Proc. IEEE Int. Conf. Robot. Automat.*, Atlanta, GA, USA, May 1993, pp. 114–120.

[11] J.-F. Wu, R. Zhang, R.-H. Wang, and Y.-X. Yao, "A systematic optimization approach for the calibration of parallel kinematics machine tools by a laser tracker," *Int. J. Mach. Tools Manuf.*, vol. 86, pp. 1–11, Nov. 2014.

[12] A. Frisoli, M. Solazzi, D. Pellegrinetti, and M. Bergamasco, "A new screw theory method for the estimation of position accuracy in spatial parallel manipulators with revolute joint clearances," *Mech. Mach. Theory*, vol. 46, pp. 1929–1949, Dec. 2011.

[13] C. Li, Y. Wu, H. Löwe, and Z. Li, "POE-based robot kinematic calibration using axis configuration space and the adjoint error model," *IEEE Trans. Robot.*, vol. 32, no. 5, pp. 1264–1279, Oct. 2016.

[14] Y. Song, J. Zhang, B. Lian, and T. Sun, "Kinematic calibration of a 5-DoF parallel kinematic machine," *Precis. Eng.*, vol. 45, pp. 242–261, Jul. 2016.

[15] H. Wang, T. Gao, J. Kinugawa, and K. Kosuge, "Finding measurement configurations for accurate robot calibration: Validation with a cable-driven robot," *IEEE Trans. Robot.*, vol. 33, no. 5, pp. 1156–1169, Oct. 2017.

[16] R. He, Y. Zhao, S. Yang, and S. Yang, "Kinematic-parameter identification for serial-robot calibration based on POE formula," *IEEE Trans. Robot.*, vol. 26, no. 3, pp. 411–423, Jun. 2010.

[17] P. Huang, J. Wang, L. Wang, and R. Yao, "Kinematical calibration of a hybrid machine tool with regularization method," *Int. J. Mach. Tools Manuf.*, vol. 51, no. 3, pp. 210–220, 2011.

[18] A. Nahvi and J. M. Hollerbach, "The noise amplification index for optimal pose selection in robot calibration," in *Proc. IEEE Int. Conf. Robot. Automat.*, Minneapolis, MN, USA, Apr. 1996, pp. 647–654.

[19] K.-I. Lee and S.-H. Yang, "Robust measurement method and uncertainty analysis for position-independent geometric errors of a rotary axis using a double ball-bar," *Int. J. Precis. Eng. Manuf.*, vol. 14, no. 2, pp. 231–239, Feb. 2013.

[20] G. Chen, H. Wang, and Z. Lin, "Determination of the identifiable parameters in robot calibration based on the POE formula," *IEEE Trans. Robot.*, vol. 30, no. 5, pp. 1066–1077, Oct. 2014.

[21] T. Sun, Y. Zhai, Y. Song, and J. Zhang, "Kinematic calibration of a 3-DoF rotational parallel manipulator using laser tracker," *Robot. Comput.-Integr. Manuf.*, vol. 41, pp. 78–91, Oct. 2016.

[22] Y. Jiang, T. Li, L. Wang, and F. Chen, "Kinematic error modeling and identification of the over-constrained parallel kinematic machine," *Robot. Comput. Integr. Manuf.*, vol. 49, pp. 105–119, Feb. 2018.

[23] X. Kong and C. M. Gosselin, "Type synthesis of 3-DOF translational parallel manipulators based on screw theory," *ASME J. Mech. Des.*, vol. 126, no. 1, pp. 83–92, Mar. 2004.

[24] *TwinCAT 3—Extended Automation Engineering (XAE)*. Accessed: Sep. 30, 2018. [Online]. Available: https://beckhoff.com/

[25] J. Fu, F. Gao, W. Chen, Y. Pan, and R. Lin, "Kinematic accuracy research of a novel six-degree-of-freedom parallel robot with three legs," *Mech. Mach. Theory*, vol. 102, pp. 86–102, Aug. 2016.

[26] P. T. Boggs and J. W. Tolle, "Sequential quadratic programming," *Acta Numer.*, vol. 4, pp. 1–51, Jan. 1995.

[27] W. Yan, F. Liu, C. Y. Chung, and K. P. Wong, "A hybrid genetic algorithm-interior point method for optimal reactive power flow," *IEEE Trans. Power Syst.*, vol. 21, no. 3, pp. 1163–1169, Aug. 2006.
[28] R. Y. K. Fung, J. Tang, and D. Wang, "Extension of a hybrid genetic algorithm for nonlinear programming problems with equality and inequality constraints," *Comput. Oper. Res.*, vol. 29, pp. 262–274, Mar. 2002.
[29] J. Wang and J. Guo, "Research on the base station calibration of multi-station and time-sharing measurement based on hybrid genetic algorithm," *Measurement*, vol. 94, pp. 139–148, Dec. 2016.
[30] J. Zhang, B. Lian, and Y. Song, "Geometric error analysis of an over-constrained parallel tracking mechanism using the screw theory," *Chin. J. Aeronaut.*, to be published, doi: 10.1016/j.cja.2018.08.021.

TAO SUN received the B.S. degree in mechanical design, manufacturing and automation from Shandong Jiaotong University, Jinan, China, in 2006, and the M.S. and Ph.D. degrees in mechanical design and theory from Tianjin University, Tianjin, China, in 2008 and 2012, respectively. He is currently a Professor with the School of Mechanical Engineering, Tianjin University.

He has authored over 60 international journal papers and over 30 authorized inventions. His research interests include mechanisms and robotics, orthopedic medical robot, and bio-inspired robot.

BINBIN LIAN received the B.S., M.S., and Ph.D. degrees from the School of Mechanical Engineering, Tianjin University, Tianjin, China, in 2010, 2012, and 2017, respectively. She joined the Mechatronics and Embedded Control System Division, Department of Machine Design, KTH Royal Institute of Technology, Stockholm, Sweden, in 2017, where she is currently a Post-Doctoral Researcher.

Her research interests include optimal control of mechatronic system, mechanisms, and robotics.

JIATENG ZHANG received the B.S. and M.S. degrees in mechanical engineering from Tianjin University, Tianjin, China, in 2011 and 2014, respectively, where he is currently pursuing the Ph.D. degree with the School of Mechanical Engineering.

His research interests include accuracy analysis, kinematic calibration, and flexible dynamics analysis of parallel robots.

YIMIN SONG received the B.S., M.S., and Ph.D. degrees in mechanical engineering from Tianjin University, Tianjin, China, in 1993, 1996, and 1999, respectively. He is currently a Professor with the School of Mechanical Engineering, Tianjin University.

He has authored over 100 journal articles and over 50 inventions. His research interests include mechanisms and robotics, mechanical dynamics, and mechanical transmission.